Balitsky-Fadin-Kuraev-Lipatov approximation versus $O(\alpha_s^3)$ corrections to large-rapidity dijet production

Vittorio Del Duca

Deutsches Elektronen-Synchrotron, DESY, D-22607 Hamburg, Germany

Carl R. Schmidt

Santa Cruz Institute for Particle Physics, University of California, Santa Cruz, California 95064

We examine dijet production at large rapidity intervals at Fermilab Tevatron energies by comparing an exact $O(\alpha_s^3)$ calculation with the Balitsky-Fadin-Kuraev-Lipatov (BFKL) approximation, which resums the leading powers of the rapidity interval y to all orders in α_s. We analyze the dependence of the exact $O(\alpha_s^3)$ calculation on the jet cone size as a function of y, and use this cross section to define an "effective rapidity" $\hat{y}$ which reduces the error that the large-y approximation induces on the kinematics. Using $\hat{y}$ in the BFKL resummation, we reexamine jet production at large transverse momenta and the transverse momentum decorrelation of the tagging jets. We find less dramatic, but still significant, effects than found previously using the large-y approximation.

I. INTRODUCTION

The state of the art in jet physics at hadron colliders is described by next-to-leading-order QCD parton-level calculations. These consist of $O(\alpha_s^2) + O(\alpha_s^3)$ one-loop $2 \to 2$ parton scattering, combined with $O(\alpha_s^3)$ tree-level $2 \to 3$ parton scattering [1]. These perturbative calculations describe the hard part of the scattering, while nonperturbative effects are factorized into the parton structure functions. An advantage of going to next-to-leading order is that it reduces the dependence on the arbitrary scale associated with this factorization. In addition, the inclusion of a third final-state parton allows a more detailed description of the jet structure. These next-to-leading-order calculations [2–4] appear to be in very good agreement with the one- and two-jet inclusive distributions obtained from the data of the Collider Detector at Fermilab (CDF) experiment at the Fermilab Tevatron collider [5, 6].

Despite these successes, it is possible to imagine kinematic configurations where this fixed-order analysis is inadequate, even though the underlying process is still perturbative in the usual sense. This could occur when the cross section contains logarithms of large ratios of kinematic invariants. Typical invariants are the hadron-hadron center-of-mass energy $\sqrt{s}$, the parton-parton center-of-mass energy $\sqrt{\hat{s}} = \sqrt{x_A x_B s}$, where x_A and x_B are the momentum fractions of the partons originating the hard scattering, and the momentum transfer Q, which is of the order of the transverse momentum of the jets produced in the hard scattering. Large logarithms will appear when $\sqrt{s} \gg Q$, in the *semihard region* of kinematic phase space. We can then avoid complications associated with the small-x behavior of the structure functions by requiring that the parton momentum fractions x_A and x_B be sufficiently large, as originally suggested by Mueller and Navelet [7]. In this case the large logarithms $\ln(\hat{s}/Q^2)$ factorize entirely into the partonic sub-

process cross section. These logarithms, which are of the size of the rapidity interval in the scattering process, can be resummed by using the techniques of Balitsky, Fadin, Kuraev, and Lipatov (BFKL) [8]. For jet events with a large rapidity interval, the amplitudes are dominated by contributions from multiple gluons that uniformly fill the interval between the two extreme jets. BFKL theory systematically resums these leading powers in the rapidity interval, including both real and virtual gluon corrections.

In a previous paper [9] we showed how to analyze dijet production experimentally so that it most closely resembles the configuration assumed in BFKL theory. The main difference from the standard hadronic jet analysis is that the jets are ordered first by their rapidity rather than by their energy. Thus, we look at all the jets in the event that are above a transverse momentum cutoff $p_{\perp \min}$, using some jet-definition algorithm, and rank them by their rapidity. We then tag the two jets with the largest and smallest rapidity and observe the distributions as a function of these two *tagging jets*. The cross section is inclusive so that the distributions are affected by the hadronic activity in the rapidity interval y between the tagging jets, whether or not these hadrons pass the jet-selection criteria. We will refer to these hadrons in the rapidity interval as *minijets*.

In Ref. [9] we showed that the exponential enhancement with the rapidity interval y in dijet production at fixed x_A and x_B, which was originally suggested as a signature of the BFKL minijets by Mueller and Navelet, is highly suppressed by the parton distribution functions at Tevatron energies. However, other observables such as the jet transverse momentum distribution, and the jet-jet correlations in $p_\perp$ and azimuthal angle are significantly affected by the minijets. For instance, the transverse momentum distribution was considerably enhanced at large $p_\perp$ and large y. This enhancement has been seen in the CDF data [6], although the data analysis differs

somewhat from that needed to compare directly with the BFKL resummation. In addition, there should be some dependence on the cutoff $p_{\perp \min}$, and we shall see here that the $p_\perp$ distributions should differ for the two tagging jets if they are not symmetrically placed around zero rapidity. Finally, we saw that the correlation in transverse momentum and azimuthal angle of the tagging jets is not a leading feature of the expansion in the rapidity interval. Accordingly, it fades away as the rapidity interval increases. The decorrelation in azimuthal angle has also been noted by Stirling [10].

For the most part these effects at large y can be easily understood in terms of the sharing of the total $\mathbf{p}_\perp$ by the additional minijets, which the BFKL resummation automatically includes. In a fixed-order calculation the effects arise first at $O(\alpha_s^3)$, where the introduction of a third final-state parton removes some of the correlations inherent at lowest order. Thus, it is interesting to compare the BFKL resummation directly with the $O(\alpha_s^3)$ result. This was done for the case of the ϕ distribution in Ref. [10]. Here we shall extend this comparison, which can be approached in two different ways. First, one can truncate the BFKL solution at $O(\alpha_s^3)$ and compare this with the exact $O(\alpha_s^3)$ result. The truncated $O(\alpha_s^3)$ BFKL cross section is just the large-y limit of the complete $O(\alpha_s^3)$ cross section, and so this comparison will indicate how good the leading logarithm approximation is at the different experiments. Second, one can compare the full BFKL solution with its truncation to $O(\alpha_s^3)$. This should give an indication of the size of the contributions from higher orders in α_s. In addition it will help to isolate the distributions which are sensitive to the resummation effects beyond next-to-leading order.

The remainder of this paper is as follows. In Sec. II we discuss the BFKL solution and its truncation to $O(\alpha_s^3)$. For illustrative purposes we also show how this second cross section is obtained from the $O(\alpha_s^3)$ tree-level $2 \to 3$ cross section in the limit of large y. In Sec. III we discuss the infrared singularities that occur at $O(\alpha_s^3)$ in order to further elucidate the approximations used in the BFKL analysis. We also observe the dependence on the jet cone size as a function of y. In Sec. IV we compare the BFKL solution truncated to $O(\alpha_s^3)$ with the exact $2 \to 3$ $O(\alpha_s^3)$ cross section. We isolate the primary contribution to the discrepancy between the two as arising from approximations used in the parton distribution functions. In Sec. V we introduce an "effective rapidity" variable to use in the BFKL formula which accounts for this difference. In particular, the effective rapidity is defined so that the truncation of the BFKL solution to $O(\alpha_s^3)$ equals the exact $2 \to 3$ $O(\alpha_s^3)$ cross section. We use this modified BFKL cross section to study the various dijet distributions, which show less dramatic, but still noticeable, effects than in Ref. [9]. In Sec. VI we present our conclusions.

II. MINIJET RESUMMATION AND $O(\alpha_s^3)$ CROSS SECTION AT LARGE RAPIDITIES

We are interested in the semi-inclusive production of two jets in hard QCD scattering. For definiteness we

will consider the scattering process $p_A \bar{p}_B \to j_1 j_2 + X$ such as at the Tevatron, but the same analysis can also be applied to photoproduction at the DESY ep collider HERA [11]. We describe the two partonic tagging jets by their transverse momenta and rapidities ($\mathbf{p}_{1\perp}, y_1$) and ($\mathbf{p}_{2\perp}, y_2$), where we always take $y_1 > y_2$. For large rapidity intervals, $y = y_1 - y_2$, the cross section for this process can be written

$$\frac{d\sigma_0}{dp_{1\perp}^2 dp_{2\perp}^2 d\phi dy_1 dy_2} = x_A^0 x_B^0 \, f_{\text{eff}}(x_A^0, \mu^2) f_{\text{eff}}(x_B^0, \mu^2)$$

$$\times \frac{d\hat{\sigma}_{gg}}{dp_{1\perp}^2 dp_{2\perp}^2 d\phi} , \qquad (1)$$

where the parton momentum fractions are dominated by the contribution from the two tagging jets,

$$x_A^0 = \frac{p_{1\perp} e^{y_1}}{\sqrt{s}},$$

$$x_B^0 = \frac{p_{2\perp} e^{-y_2}}{\sqrt{s}}, \qquad (2)$$

and μ is the factorization and/or renormalization scale. In this limit the amplitude is dominated by gg, qg, and qq scattering diagrams with gluon exchange in the t channel. The relative magnitude of the different subprocesses is fixed by the color strength of the respective jet-production vertices, and so it suffices to consider only gg scattering and to include the other subprocesses by means of the effective parton distribution function [12]

$$f_{\text{eff}}(x, \mu^2) = G(x, \mu^2) + \frac{C_F}{C_A} \sum_f [Q_f(x, \mu^2) + \bar{Q}_f(x, \mu^2)] .$$

$$(3)$$

In (3) the sum is over the quark flavors, $C_A = N_c = 3$, is the Casimir operator of the adjoint representation and $C_F = (N_c^2 - 1)/2N_c = 4/3$ is the one of the fundamental representation.

The higher-order corrections to the gg subprocess cross section in (1) can be expressed via the solution of the BFKL equation [8], which is an all-order resummation in α_s of the leading powers of the rapidity interval,

$$\frac{d\hat{\sigma}_{gg}}{dp_{1\perp}^2 dp_{2\perp}^2 d\phi} = \frac{C_A^2 \alpha_s^2}{4\pi p_{1\perp}^3 p_{2\perp}^3} \sum_n e^{in(\phi - \pi)}$$

$$\times \int_0^\infty d\nu e^{\omega(n,\nu) y} \cos\left(\nu \ln \frac{p_{1\perp}^2}{p_{2\perp}^2}\right), \qquad (4)$$

with

$$\omega(n, \nu) = \frac{2C_A \alpha_s}{\pi} \left[\psi(1) - \text{Re}\,\psi\left(\frac{|n| + 1}{2} + i\nu\right) \right],$$

$$(5)$$

and ψ the logarithmic derivative of the Γ function. Equation (4) can be expanded order by order in α_s and compared with a fixed-order calculation of dijet production at the same order of α_s, in the large rapidity limit [10]. By expanding the exponential in (4) to zeroth order in α_s we obtain the tree-level large-y cross section

$$\frac{d\hat{\sigma}_{gg}^{(0)}}{dp_{1\perp}^2 dp_{2\perp}^2 d\phi} = \frac{\pi C_A^2 \alpha_s^2}{2p_{1\perp}^4} \delta(p_{1\perp}^2 - p_{2\perp}^2)\, \delta(\phi - \pi)\ . \quad (6)$$

At $O(\alpha_s)$ in the exponential we obtain

$$\frac{d\hat{\sigma}_{gg}^{(1)}}{dp_{1\perp}^2 dp_{2\perp}^2 d\phi} = \frac{C_A^2 \alpha_s^2}{4\pi p_{1\perp}^3 p_{2\perp}^3} \sum_n e^{in(\phi - \pi)}$$

$$\times \int_0^\infty d\nu \frac{2C_A \alpha_s}{\pi} y \left[\psi(1) - \mathrm{Re}\, \psi \right.$$

$$\left. \times \left(\frac{|n| + 1}{2} + i\nu \right) \right] \cos\left(\nu \ln \frac{p_{1\perp}^2}{p_{2\perp}^2} \right)\ .$$

$$(7)$$

When $p_{1\perp} \neq p_{2\perp}$ we can integrate out ν and sum explicitly over n, by using the integral representation of the ψ function:

$$\psi(z) = \int_0^1 dx\, \frac{1 - x^{z-1}}{1 - x}\ -\ \gamma, \quad (8)$$

with the Euler constant $\gamma = 0.577215\ldots$. We obtain

$$\frac{d\hat{\sigma}_{gg}^{(1)}}{dp_{1\perp}^2 dp_{2\perp}^2 d\phi} = \frac{C_A^2 \alpha_s^2}{4\pi p_{1\perp}^2 p_{2\perp}^2}\, \frac{C_A \alpha_s y}{p_{1\perp}^2 + p_{2\perp}^2 + 2p_{1\perp} p_{2\perp} \cos\phi}\ . \quad (9)$$

When $p_{1\perp} \sim p_{2\perp}$ the cross section (7) is dominated by configurations where the third parton is soft. These infrared singularities are regulated by the BFKL solution, which includes both real and virtual corrections. To see how this occurs we can integrate (7) over $p_{2\perp}^2$ in the interval defined by $|p_{1\perp}^2 - p_{2\perp}^2| < \epsilon p_{1\perp}^2$, for ϵ sufficiently small. The integrals over ν and x can be performed, and the series in n can be summed, giving a finite answer:

$$\frac{d\hat{\sigma}_{gg}^{(1)}}{dp_{1\perp}^2 d\phi} = \frac{\pi C_A^2 \alpha_s^2}{2p_{1\perp}^4} \delta(\phi - \pi)\, \frac{2C_A \alpha_s}{\pi} y \ln \epsilon, \quad (10)$$

up to terms of $O(\epsilon)$. For sufficiently small ϵ this configuration is indistinguishable from a configuration with only two final-state partons. Thus, for $|p_{1\perp}^2 - p_{2\perp}^2| < \epsilon p_{1\perp}^2$ we can write the cross section to $O(\alpha_s^3)$ as

$$\frac{d\hat{\sigma}_{gg}^{(0+1)}}{dp_{1\perp}^2 dp_{2\perp}^2 d\phi} = \frac{\pi C_A^2 \alpha_s^2}{2p_{1\perp}^4} \delta(p_{1\perp}^2 - p_{2\perp}^2)\, \delta(\phi - \pi)$$

$$\times \left(1 + \frac{2C_A \alpha_s}{\pi} y \ln \epsilon \right)\ . \quad (11)$$

For $|p_{1\perp}^2 - p_{2\perp}^2| > \epsilon p_{1\perp}^2$ we can use Eq. (9). Combining these two formulas (11) and (9), the dependence on the unphysical variable ϵ will vanish in any inclusive process integrated over a range of momenta, for small enough ϵ.

It is also informative to derive the $2 \to 3$ cross section (9) by taking the large-rapidity limit of the $O(\alpha_s)$ real corrections to gluon-gluon scattering, computed in the conventional way [13]. First, note that in the large-rapidity limit the leading contribution is given by the $gg \to ggg$ subprocess, the diagrams with final-state

quarks being subleading. The squared scattering amplitude for this, summed (averaged) over final (initial) colors and helicities, is given in Ref. [14] as

$$|M|^2 = 4\, (\pi\alpha_s C_A)^3$$

$$\times \sum_{i>j} s_{ij}^4 \sum_{[A,1,2,3,B]'} \frac{1}{s_{A1} s_{12} s_{23} s_{3B} s_{AB}}, \quad (12)$$

with $i, j = A, 1, 2, 3, B$, and with the second sum over the noncyclic permutations of the set $[A, 1, 2, 3, B]$. The kinematic invariants are defined here by

$$s_{AB} = \hat{s} = x_A x_B s = \sum_{i,j=1}^3 p_{i\perp} p_{j\perp} e^{y_i - y_j},$$

$$s_{A,i} = -\sum_{j=1}^3 p_{i\perp} p_{j\perp} e^{-(y_i - y_j)}, \quad (13)$$

$$s_{B,i} = -\sum_{j=1}^3 p_{i\perp} p_{j\perp} e^{y_i - y_j},$$

$$s_{ij} = 2p_{i\perp} p_{j\perp} \left[\cosh(y_i - y_j) - \cos(\phi_i - \phi_j) \right].$$

In the large-rapidity limit Eq. (12) becomes [15]

$$|M|^2 = 128\, (\pi\alpha_s C_A)^3\, \frac{\hat{s}^2}{p_{1\perp}^2 p_{2\perp}^2 p_{3\perp}^2}. \quad (14)$$

The large-rapidity limit of the phase space for three-particle production is

$$d\Pi_3 = \frac{1}{2\hat{s}} \frac{dy_3}{4\pi} \left(\prod_{i=1}^3 \frac{d^2 p_{i\perp}}{(2\pi)^2} \right) (2\pi)^2 \delta^2 \left(\sum_{i=1}^3 p_{i\perp} \right), \quad (15)$$

where we have fixed the rapidities of the two gluons at largest and smallest rapidity and y_3 is the rapidity of the third gluon. Using the amplitude (14), the phase space (15), and the appropriate flux factor, we obtain for the dijet production cross section $d\hat{\sigma}_{gg}/dp_{1\perp}^2 dp_{2\perp}^2 d\phi$ the same expression as the one obtained in Eq. (9) via the expansion of the BFKL solution. Note that the overall factor of y in Eq. (9) comes from the integration of the rapidity of the third final-state gluon over the interval spanned by the tagging gluons.

III. COLLINEAR SINGULARITIES IN DIJET PRODUCTION

Before entering the details of a comparison between the BFKL resummation and the complete $O(\alpha_s^3)$ result, it is useful to consider the infrared singularities that occur in the two approximations to dijet production. These singularities depend on the geometry of the event and thus are sensitive to how dijet production is defined. In the next-to-leading-order (NLO) approximation the phase space integration over the kinematic variables of the third (unresolved) parton generates infrared singularities when it becomes soft and collinear singularities when it becomes collinear either with the initial-state partons or with the other final-state partons. In contrast, the BFKL approximation only contains the effects of soft gluons. Because of
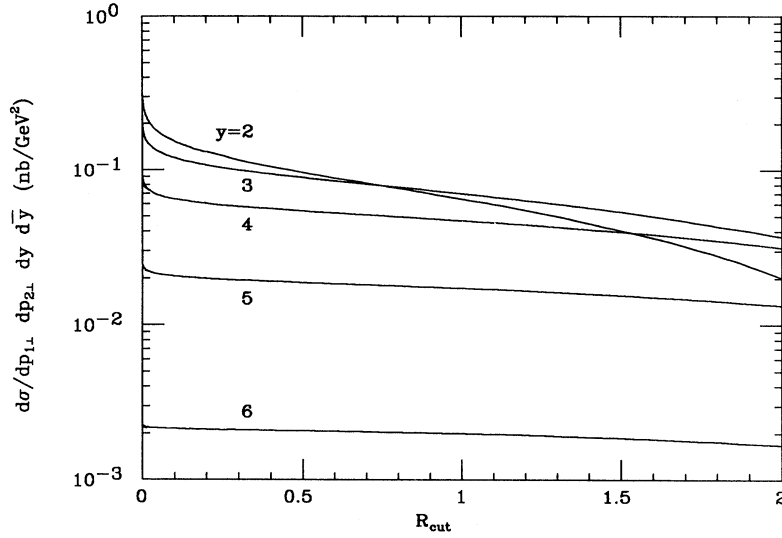
FIG. 1.   Dijet production as a function of the jet cone size $R_{\rm cut}$, at $p_{1\perp} = 20$ GeV and $p_{2\perp} = 50$ GeV, $\bar{y} = 0$ and $y = 2$, 3, 4, 5, and 6.

the explicit rapidity ordering, the unresolved partons are bound to lie within the rapidity interval defined by the tagging jets, and so can never become collinear with the initial-state partons.[1] In addition, in the large-rapidity limit the region of phase space where the third parton becomes collinear with either of the other final-state partons gives a nonleading contribution.

Let us examine this last point further. First we recall the standard definition of a jet as consisting of all the partons lying within a circle of radius $R_{\rm cut} = [(y_J - y)^2 + (\phi_J - \phi)^2]^{1/2}$ from the jet axis (y_J, ϕ_J) in the plane defined by rapidity and azimuthal angle (i.e., the lego plot). Then we look at the dependence on the jet cone size $R_{\rm cut}$ of the $O(\alpha_s^3)$ corrections to dijet production. Namely, we consider in Fig. 1 the contribution of the three-jet configurations, computed through the $2 \to 3$ parton amplitudes, to the cross section

$$\frac{d\sigma}{dy\, d\bar{y}\, dp_{1\perp}\, dp_{2\perp}}$$

$$= \int_{y_2}^{y_1} dy_3 \int d\phi \sum_{ij} x_A x_B\, f_{i/A}(x_A, \mu^2) f_{j/B}(x_B, \mu^2)$$

$$\times \frac{|M_{ij}|^2 p_{1\perp} p_{2\perp}}{128 \pi^4 \hat{s}^2}, \tag{16}$$

as a function of the jet cone size $R_{\rm cut}$ at different values of the rapidity interval y. $f_{i(j)} = Q, \bar{Q}, G$ labels the distribution function of the parton species and flavor i $(j) = q, \bar{q}, g$ inside hadron A (B). We include all parton

---

[1]Of course, it is always possible for a parton or jet to be produced outside of the rapidity interval of the tagging jets, but to go undetected because it has too small $p_{i\perp}$ or too large $|y_i|$. In the context of the BFKL approximation this jet would be considered part of the evolution of the structure functions, and would not be included in the calculation of the parton subprocess.

subprocesses [13], and use the exact values of the parton momentum fractions

$$x_A = \frac{p_{1\perp} e^{y_1} + p_{2\perp} e^{y_2} + p_{3\perp} e^{y_3}}{\sqrt{s}},$$

$$x_B = \frac{p_{1\perp} e^{-y_1} + p_{2\perp} e^{-y_2} + p_{3\perp} e^{-y_3}}{\sqrt{s}}. \tag{17}$$

As in our previous analysis [9] we set the rapidity boost $\bar{y} = (y_1 + y_2)/2 = 0$, since we are mainly interested in the behavior of the parton subprocess, which does not depend on $\bar{y}$. We fix the transverse momenta of the tagging jets at different values $p_{1\perp} = 20$ GeV and $p_{2\perp} = 50$ GeV in order to ensure that the third parton cannot become soft. Furthermore, collinear configurations where the distance R between two of the partons on the lego plot is smaller than $R_{\rm cut}$ are discarded, because the resulting "combined" jet would be back to back with the remaining parton and have the same $p_\perp$ as it. Finally, in the spirit of the BFKL approximation, we restrict the rapidity of the third parton to lie between the two tagging jets. Note that this last approximation differs from the full NLO treatment which includes initial-state collinear radiation and uses the Altarelli-Parisi subtraction to handle the divergences. Therefore, in this calculation and in all BFKL calculations, the parton density functions should be treated at leading order (LO) and will have all the associated LO factorization-scale dependence. In all of our plots we use the LO CTEQ collaboration parton distribution functions [16] with the renormalization and factorization scales set to the geometric mean of the transverse momenta of the tagging jets $\mu^2 = p_{1\perp} p_{2\perp}$. As Fig. 1 shows, the dependence of the dijet production on the jet cone size $R_{\rm cut}$ decreases as y is increased. At $y = 6$ the tagging jets are so widely separated in rapidity that there is almost no dependence on $R_{\rm cut}$ at all. This confirms that the phase space region where two final-state partons are collinear is subleading at large rapidities, as suggested by BFKL theory.

IV. BFKL AND $O(\alpha_s^3)$ CORRECTIONS TO THE $p_\perp$ DISTRIBUTIONS

In Sec. II we have shown that the truncated $O(\alpha_s^3)$ BFKL contribution to dijet production is the large-rapidity limit of the complete $O(\alpha_s^3)$ corrections. Here we want to see how well this works in practice in the jet-jet $p_\perp$ correlation case examined in Ref. [9]. In Fig. 2 we consider the contribution of the three-jet amplitudes to the $p_\perp$ correlation $d\sigma/dy\,d\bar{y}\,dp_{1\perp}\,dp_{2\perp}$, plotted as a function of the transverse momentum $p_{1\perp}$, at a fixed value of $p_{2\perp} = 50$ GeV and at $y = 2$ and 6. The customary value for the jet cone size $R_{\mathrm{cut}} = 0.7$ has been used. As in Fig. 1, configurations where the distance R between two partons on the lego plot is smaller than R_{cut} are discarded, since they would be counted as a two-jet event with $p_{1\perp} = p_{2\perp}$. We go from the exact configurations to the large-y approximation to them in three steps. The dashed curves are computed through the exact 2→3 parton amplitudes [13] and kinematics (17), the dotted curves through the large-y parton amplitudes (14) and the exact kinematics (17), and the solid curves through the large-y parton amplitudes (14) and kinematics (2). As the plots show, the error in using the large-y approximation grows with the imbalance in transverse momentum of the tagging jets. While at small y's the error is distributed between the approximation on the amplitudes and the one on the parton distribution functions, at large y's most of the error comes in using the large-y approximation in the parton distribution functions. We have also made this comparison for the larger rapidity intervals obtainable at the CERN Large Hadron Collider (LHC) and have found that this discrepancy, although smaller, is not insignificant.

This discrepancy can be understood by recalling that the rapidity y_3 of the third jet is integrated over the full range of the interval from y_2 to y_1. If we neglect its contribution to the momentum fractions as in (2), this just multiplies the cross section by a factor of y as in Eq. (9). However, Eq. (2) can be a bad approximation to the ex-

act kinematics (17) over much of the integral if $p_{3\perp}$ is not small. For y_3 near the extremes, using the exact kinematics in the parton distribution functions produces a large suppression, so that the "effective" rapidity range of y_3 is reduced substantially. The truncated $O(\alpha_s^3)$ BFKL (solid) curve neglects this effect, and so it overestimates the cross section. Note, however, that near $p_{1\perp} = p_{2\perp}$ the transverse momentum of the third parton is small, and so its contribution to the x's in (17) can be safely neglected.

V. EFFECTIVE RAPIDITY INTERVAL

We have just seen in the previous section that the large-y approximation used in the BFKL resummation seriously overestimates the cross section when the two tagging jets have unequal energies, even for rapidity intervals as large as $y = 6$. This occurs because the large-y cross section (9) assumes that the third (minijet) parton can be produced anywhere within the rapidity interval $[y_2, y_1]$ with equal probability, whereas in the full $2 \to 3$ cross section the probability is highly suppressed by the structure functions when the third jet strays too far from the center of this interval. In this section we will attempt to fix this problem by including this suppression effect directly into the BFKL equation.

The BFKL solution as presented in Eq. (4) is an all-orders resummation in $\alpha_s y$ where y is the kinematic rapidity interval defined by the tagging jets. However, to be completely precise, the rapidity variable which is resummed by BFKL is only defined up to transformations $y \to y + X$ where X is subleading at large rapidities. This is analogous to a change in the scale Q^2 in the standard $\alpha_s \ln(Q^2)$ resummation, and in the same way that one chooses a physical value of Q^2 to lessen the effects of nonleading terms in this resummation, one can choose a more physical rapidity variable in the BFKL resummation. From the results of the previous section we see that a better rapidity variable would be one that reflects the range in rapidity spanned by the minijets, which is
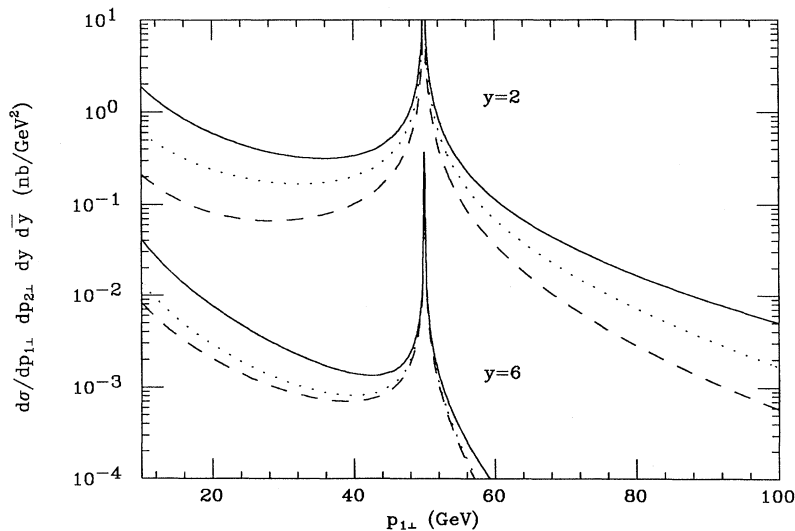
FIG. 2. $p_\perp$ distribution of jet 1 with the jet 2 transverse momentum fixed at 50 GeV, at $\bar{y} = 0$ and at $y = 2$ and 6. The jet cone size is fixed at 0.7. The dashed curves are computed through the exact 2→3 parton amplitudes and kinematics, the dotted curves through the large-y parton amplitudes and the exact kinematics, and the solid curves through the large-y parton amplitudes and kinematics.

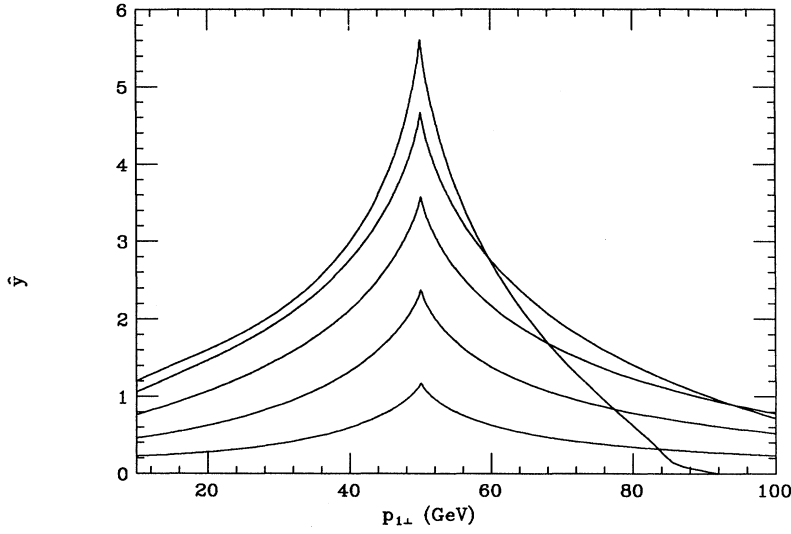FIG. 3. $\hat{y}$ as a function of $p_{1\perp}$ for fixed $p_{2\perp} = 50$ GeV and $n = 0$, $\bar{y} = 0$. The curves from bottom to top are for $y = 2, 3, 4, 5$, and 6. The jet cone size is fixed at 0.7. The upper end of the curve $y = 6$ is cut off because $p_{1\perp}$ reaches the kinematic limit.

typically less than the kinematic rapidity interval y. Let us define an "effective rapidity" $\hat{y}(n, p_{1\perp}, p_{2\perp}, \bar{y}, y)$ by

$$\hat{y} \equiv y \, \frac{\int d\phi \, \cos(n\phi) \, \left(d\sigma/dyd\bar{y}dp_{1\perp}dp_{2\perp}d\phi\right)}{\int d\phi \, \cos(n\phi) \, \left(d\sigma_0/dyd\bar{y}dp_{1\perp}dp_{2\perp}d\phi\right)} \, , \quad (18)$$

where n is the Fourier series index of Eq. (4). The cross section in the numerator is that of Eq. (16) and is computed using the exact kinematics (17), while the cross section in the denominator is that of Eq. (1) and is computed using the large-y kinematics (2). The denominator can easily be computed analytically using the large-y solution (9). Note that $\hat{y}$ is defined so that if we replace $y \to \hat{y}$ in the BFKL solution (4) and truncate to $O(\alpha_s^3)$ we recover the exact $2 \to 3$ cross section. Also note that asymptotically for large y, the difference $y-\hat{y}$ is nonleading. Thus, we can use $\hat{y}$ in (4) and obtain a quantitatively more reliable solution.

In Fig. 3 we plot $\hat{y}$ as a function of $p_{1\perp}$ for $n = 0$, $p_{2\perp} = 50$ GeV, $\bar{y} = 0$, and $y = 2, 3, 4, 5, 6$ with $R_{\rm cut} = 0.7$. For $y = 2$ and 6 this is just given by the ratio of the dashed curves to the solid curves in Fig. 2, multiplied by y. Near $p_{1\perp} = p_{2\perp}$, $\hat{y}$ approaches the kinematic rapidity y, especially for large y, but it falls quickly as the two jets move apart in transverse momentum. Thus, we would expect the effects of the resummation to be most important near $p_{1\perp} = p_{2\perp}$. We can see this clearly in the jet-jet $p_\perp$ correlation plot of Fig. 4, where we compare the exact $2 \to 3$ $O(\alpha_s^3)$ cross section (dashed curve) with the BFKL resummation using $\hat{y}$ (solid curve). As in Fig. 2 we fix $p_{2\perp} = 50$ GeV, $\bar{y} = 0$, and plot as a function of $p_{1\perp}$ for $y = 2$ and 6, using a jet cone size of $R_{\rm cut} = 0.7$. In this and in the plots that follow, $\hat{y}$ is fixed at $n = 0$ by the integration over the azimuthal angle ϕ. As expected, for $y = 2$ there is little difference between the two approximations. For $y = 6$ the higher orders of the BFKL resummation are very important near $p_{1\perp} = p_{2\perp}$, but have less of an effect when the jets are mismatched
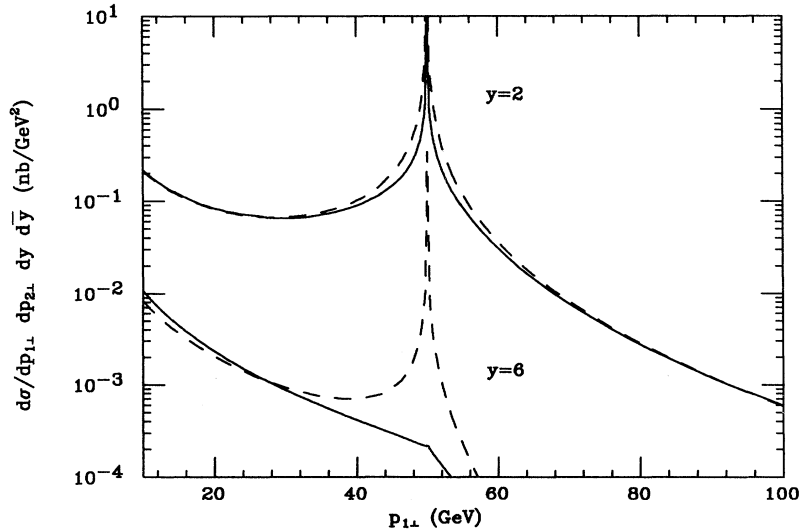

FIG. 4. $p_\perp$ distribution of jet 1 with the jet 2 transverse momentum fixed at 50 GeV, at $\bar{y} = 0$ and at $y = 2$ and 6. The jet cone size is fixed at 0.7. The dashed curves are computed through the exact $2\to3$ parton amplitudes and kinematics; the solid curves are computed from the full BFKL solution using $\hat{y}$.
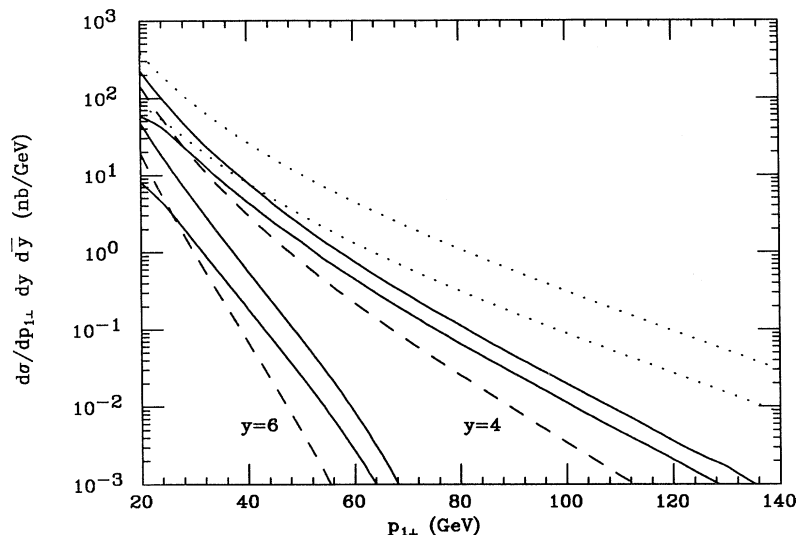
FIG. 5. $p_\perp$ distribution of jet 1 at $\bar{y} = 0$ and $y = 4$ and 6. The dashed curves are the exact Born-level $p_\perp$ distributions. The solid curves are the $p_\perp$ distributions computed using $\hat{y}$ in the BFKL resummation, with two different cutoffs for jet 2, the upper curve with $p_{2\perp min} = 10$ GeV and the lower curve with $p_{2\perp min} = 20$ GeV. The dotted curves are the $p_\perp$ distributions at $y = 4$ only, computed using the kinematic rapidity y in the BFKL resummation, with $p_{2\perp min} = 10$ GeV and 20 GeV.

in transverse momentum.

Next, in Fig. 5 we plot the transverse momentum distribution $d\sigma/dy\,d\bar{y}\,dp_{1\perp}$ of jet 1 at $y = 4$ and 6 and $\bar{y} = 0$. The dashed curves are computed through the exact Born-level matrix elements and the solid curves using $\hat{y}$ in the BFKL resummation and two different cutoffs for jet 2 transverse momentum, $p_{2\perp min} = 10$ GeV and 20 GeV. The effect of the radiative corrections is to release the $p_\perp$ distribution from the Born-level requirement that $p_{1\perp} = p_{2\perp}$. At a fixed order of α_s and for a given $p_{1\perp}$, jet 2 and the minijets try to have $p_\perp$ as small as possible in order to minimize their contribution to the x's (17) and thus maximize the value of the parton distribution functions. They are only constrained by the overall transverse momentum conservation. Eventually when the number of minijets is very high, or virtually infinite as in the BFKL resummation, the smallest value of $p_{2\perp}$ is not fixed any more by transverse momentum conservation but by the minimum $p_\perp$ experimentally attainable [9]. This explains the strong sensitivity of the curves in Fig. 5 to the value[2] of $p_{2\perp min}$. The crossing of the curves with $p_{2\perp min} = 20$ GeV below the Born curves for small values of $p_{1\perp}$ is a further manifestation of this decorrelation in transverse momentum. For $p_{1\perp} \sim 20$ GeV, jet 2 very often radiates away enough energy so that $p_{2\perp} < p_{2\perp min}$. Thus, events that would have been kept at the Born level are now discarded when higher orders are included. Finally, for sake of comparison, we replot in the dotted curves the $p_\perp$ distribution computed at $y = 4$ using y in the BFKL resummation, with $p_{2\perp min} = 10$ GeV and 20 GeV [9]. We note that, using the effective rapidity $\hat{y}$ rather than the kinematic rapidity y in the BFKL

resummation, the enhancement in the $p_\perp$ distribution is considerably reduced.

To examine further the kinematic effects on dijet production we plot in Fig. 6 the $p_\perp$ distribution at $|\bar{y}| = 2$ and $y = 4$ as a function of the transverse momentum of the jets at largest ($|y_f| = 4$) and smallest ($|y_c| = 0$) absolute rapidities, which we call the *forward* jet and the *central* jet, respectively. As in Fig. 5 we use two different cutoffs $p_{\perp min} = 10$ GeV and 20 GeV for the transverse momentum integrated out. Since we only have changed $\bar{y}$ with respect to Fig. 5 the contribution of the parton subprocess to the $p_\perp$ distribution will be the same as in Fig. 5, but the contribution of the parton distribution functions will change. The dashed curve is computed through the exact Born-level matrix elements and the dotted and solid curves using $\hat{y}$ in the BFKL resummation. At the Born level the transverse momentum distributions of the forward and central jets are the same since $p_{f\perp} = p_{c\perp}$, but they become starkly different when higher orders are included. The dotted curves are the distributions of the forward jet. They do not appreciably differ from the Born-level curve because the upper bound $p_{f\perp} < \sqrt{s}\exp(-|y_f|)$ from light-cone momentum conservation is very restrictive and the phase space of the forward jet does not basically change going from LO to higher-order corrections. On the other hand the solid curves, which represent the distributions of the central jet, show a huge enhancement and very different slopes as compared to the Born level. To understand this, we have to look at the kinematics of the higher-order corrections. At $O(\alpha_s^3)$ it is possible to let $p_{c\perp}$ grow by taking the third jet at small absolute rapidity and almost back to back with the central jet, $p_{3\perp} \simeq -p_{c\perp}$ and $y_3 \simeq 0$, while taking the forward jet as slim as possible, $p_{f\perp} \simeq p_{\perp min}$. Then from light-cone momentum conservation $p_{c\perp max} \simeq [\sqrt{s} - p_{\perp min}\exp(|y_f|)]/2$, which is much bigger than the Born-level upper bound. This picture generalizes to higher orders with the transverse momentum of the minijets balancing that of the central jet, while the forward jet is produced near $p_{\perp min}$. In order

---

[2]On the other hand, light-cone momentum conservation requires that $p_{1\perp} < \sqrt{s}\exp(-y_1)$, so that at large-rapidity intervals the maximum value of $p_{1\perp}$ does not appreciably change going from the Born level to higher-order corrections.
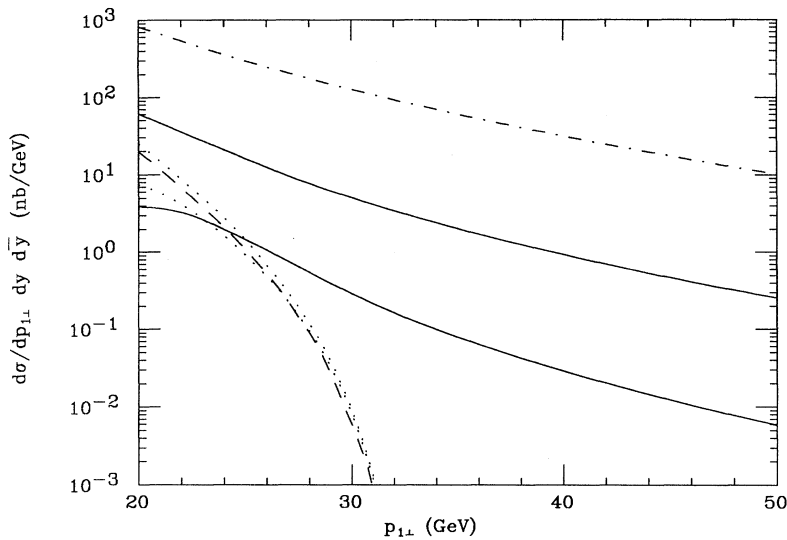
FIG. 6. $p_\perp$ distribution at $|\bar{y}| = 2$ and $y = 4$. The dashed curve is the exact Born-level $p_\perp$ distribution. The dotted (solid) curves are the $p_\perp$ distributions of the forward (central) jet computed using $\hat{y}$ in the BFKL resummation, with two different cutoffs for the transverse momentum integrated out, the upper curve with $p_{\perp min} = 10$ GeV and the lower curve with $p_{\perp min} = 20$ GeV. The dot-dashed curve is the exact Born-level $p_\perp$ distribution at $|\bar{y}| = 0.5$ and $y = 1$.

to test this picture we consider in the dot-dashed curve the transverse momentum distribution for the Born-level production of two jets in the central region $|\bar{y}| = 0.5$ and $y=1$. The slope of this curve is similar to that of the solid curves, suggesting that the $p_{c\perp}$ distribution is dominated by events with two central jets and one soft forward jet, where we tag on the forward jet and one of the central jets. In the BFKL resummation the second hard central jet is presumably replaced by a succession of minijets. Thus, it is misleading to compare the BFKL resummation to the Born level (dashed curve) for the $p_{c\perp}$ distribution, since it is dominated by events with more than two jets. A better comparison in this case would be between the BFKL resummation and a NLO calculation.

VI. CONCLUSIONS

In this paper we have attempted to better grasp the range of validity of the BFKL resummation by comparing it with an exact $2 \to 3$ $O(\alpha_s^3)$ calculation. We saw that the dependence on the jet cone size quickly becomes insignificant for moderate rapidities, just as is assumed in the BFKL formalism. However, the approximation to the kinematics in the parton momentum fractions causes a serious error in the BFKL predictions when the tagging jets are not back to back in $p_\perp$ and ϕ. In order to account for this error we introduced an effective rapidity $\hat{y}$ which restricts the phase space of the minijets in such a way that the truncation of the BFKL resummation to $O(\alpha_s^3)$ agrees with the exact $2 \to 3$ $O(\alpha_s^3)$ calculation.

Using the BFKL resummation with the effective ra-

pidity $\hat{y}$ we have seen that the effects on the $p_\perp$ spectrum are not as dramatic as we had predicted previously. The difficulty in detecting these deviations from the Born-level computation are compounded by renormalization and/or factorization scale ambiguities, which are at least as problematic here as at the Born level. Because of the two scales defined by the tagging jets we could let $\mu^2 = Cp_{1\perp}p_{2\perp}$, $C\max(p_{1\perp}^2, p_{2\perp}^2)$, or some other choice where C is some constant of order 1. Because of the relatively small deviations of the BFKL resummation with the effective rapidity $\hat{y}$ from the Born-level calculation, and the sizable renormalization and/or factorization scale ambiguities in the BFKL approximation, we expect that a complete NLO calculation could give a more reliable estimate to the raw $p_\perp$ spectra. However, we do note that much of the uncertainties due to the renormalization and/or factorization scale drop out in the ratios of cross sections so that, for instance, the predictions of the ratio of the $p_{1\perp}$ spectra with different $p_{2\perp min}$ cutoffs are probably reliable to $\sim 15\%$. In addition, the large corrections in the $p_\perp$ correlation and ϕ correlation plots suggest that a NLO calculation would be inadequate in these cases, and that the BFKL resummation using the effective rapidity $\hat{y}$ should do a better job here.

[1] R.K. Ellis and J.C. Sexton, Nucl. Phys. **B269**, 445 (1986); Z. Bern and D.A. Kosower, *ibid.* **B379**, 451 (1992); Z. Kunszt, A. Signer, and Z. Trocsanyi, *ibid.* **B411**, 397 (1994).

[2] S.D. Ellis, Z. Kunszt, and D.E. Soper, Phys. Rev. D **40**, 2188 (1989); Phys. Rev. Lett. **64**, 2121 (1990); F. Aversa,

M. Greco, P. Chiappetta, and J.Ph. Guillet, *ibid.* **65**, 401 (1990); Z. Phys. C **49**, 459 (1991).

[3] S.D. Ellis, Z. Kunszt, and D.E. Soper, Phys. Rev. Lett. **69**, 1496 (1992).

[4] W.T. Giele, E.W.N. Glover, and D.A. Kosower, Phys. Rev. Lett. **73**, 2019 (1994).

[5] CDF Collaboration, F. Abe *et al.*, Phys. Rev. Lett. **68**, 1104 (1992); CDF Collaboration, F. Abe *et al.*, *ibid.* **69**, 2896 (1992).

[6] CDF Collaboration, F. Abe *et al.*, in *Lepton and Photon Interactions*, Proceedings of the 16th International Symposium, Ithaca, New York, 1993, edited by P. Drell and D. Rubin, AIP Conf. Proc. No. 302 (AIP, New York, 1994).

[7] A.H. Mueller and H. Navelet, Nucl. Phys. **B282**, 727 (1987).

[8] L.N. Lipatov, Yad. Fiz. **23**, 642 (1976) [Sov. J. Nucl. Phys. **23**, 338 (1976)]; E.A. Kuraev, L.N. Lipatov, and V.S. Fadin, Zh. Eksp. Teor. Fiz. **71**, 840 (1976) [Sov. Phys. JETP **44**, 443 (1976)]; **72**, 377 (1977) [**45**, 199 (1977)]; Ya.Ya. Balitsky and L.N. Lipatov, Yad. Fiz.

28, 1597 (1978) [Sov. J. Nucl. Phys. **28**, 822 (1978)].

[9] V. Del Duca and C.R. Schmidt, Phys. Rev. D **49**, 4510 (1994).

[10] W.J. Stirling, Nucl. Phys. **B423**, 56 (1994).

[11] V. Del Duca and C.R. Schmidt (in preparation).

[12] B.L. Combridge and C.J. Maxwell, Nucl. Phys. **B239**, 429 (1984).

[13] T. Gottschalk and D. Sivers, Phys. Rev. D **21**, 102 (1980); Z. Kunszt and E. Pietarinen, Nucl. Phys. **B164**, 45 (1980); F.A. Berends *et al.*, Phys. Lett. **103B**, 102 (1981).

[14] S.J. Parke and T. Taylor, Phys. Rev. Lett. **56**, 2459 (1986).

[15] V. Del Duca, Phys. Rev. D **48**, 5133 (1993).

[16] J. Botts *et al.*, Phys. Lett. B **304**, 159 (1993).